Electronic Supplementary Information

Sonochemical regulation of oxygen vacancy for Bi_2WO_6 nanosheets-based photoanode to promote photoelectrochemical performance

Ruowen Zhao, [a] *Yupu Zhang,* [a] *Fangli Wu,* [a] *Jianyuan Wang,* [a] *Fang Chen*[*a] *and Wei Zhai*[*a]

[a]MOE Key Laboratory of Materials Physics and Chemistry under Extraordinary Conditions, Northwestern Polytechnical University, Xi'an, 710072, China

[*]E-mail: chenfang820811@nwpu.edu.cn; zhaiwei322@nwpu.edu.cn

Synthesis of BiOI nanosheet arrays:

BiOI nanosheets arrays were synthesized on fluorine-doped tin oxide (FTO) by cathodic deposition method. The precursor solution was prepared by dissolving 0.98 g $Bi(NO_3)_3 \cdot 5H_2O$ in 50 mL 0.4 M KI solution and adding HNO_3 to adjust the pH value to 1.7, which was further added to 20 mL 0.23 M p-benzoquinone ethanol solution and mixed well. The electrodeposition process was proceeded in a three-electrode electrolytic device. FTO (1.5×2.5 cm^2) was used as the working electrode, Pt foil net (0.5×0.5 cm^2) was used as the counter electrode, a saturated Ag/AgCl (4 M KCl) was used as the reference electrode and the constant potential was set as -0.1 V vs Ag/AgCl, the deposition process lasted for 130 s. Finally, the two-dimensional BiOI nanosheet arrays were obtained.

Conversion between SCE and RHE:

The conversion between potentials versus SCE and versus Reversible Hydrogen Electrode (RHE) is performed using Eq. 1-2:

$$E_{RHE} = E_{SCE(reference)} + E_{SCE} + 0.0591 \times pH \quad (1)$$

$$E_{SCE(reference)} = 0.024V \text{ vs. NHE at } 25°C \quad (2)$$

where pH is a pH value of the electrolyte.

Tabel S1. Reaction conditions of BWO and BWO-ux (x=0, 1, 2, 3 and 3') photoanodes.

Sample	Input ultrasonic power (w)	Reaction solution
BWO	0	No
BWO-u0	0	NaOH
BWO-u1	90	NaOH
BWO-u2	360	NaOH
BWO-u3	630	NaOH
BWO-u3'	630	NaOH+IPA(5%)

*The concentration of NaOH and IPA in reaction solution are 0.25 mol/L and 0.66 mol/L (99.9%), respectively. The ultrasonic time maintain 10 min in all samples.

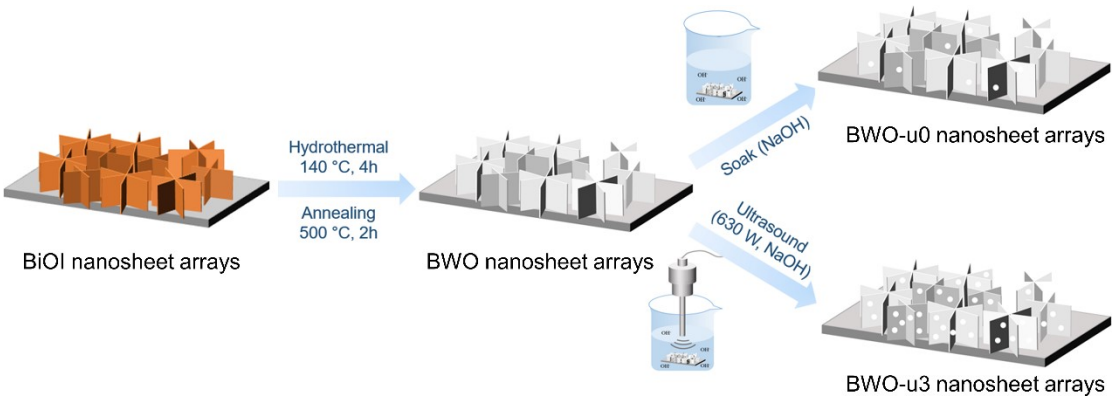

Fig. S1 Synthesis procedure of BWO, BWO-u0 and BWO-u3 nanosheets-based photoanodes.

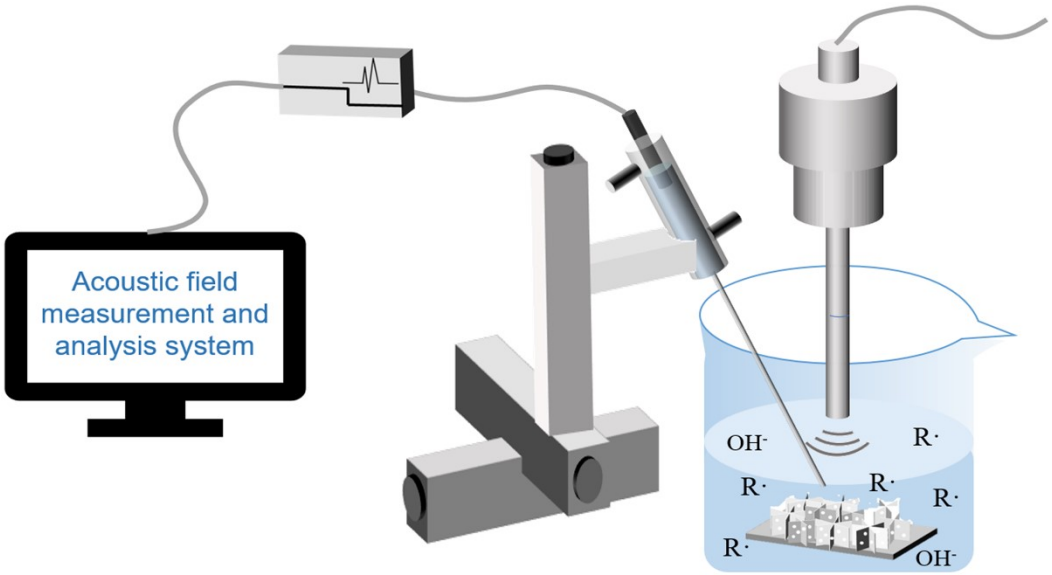

Fig. S2 Testing device of transient (and stable) cavitation intensity (W/m^2) spectrum.

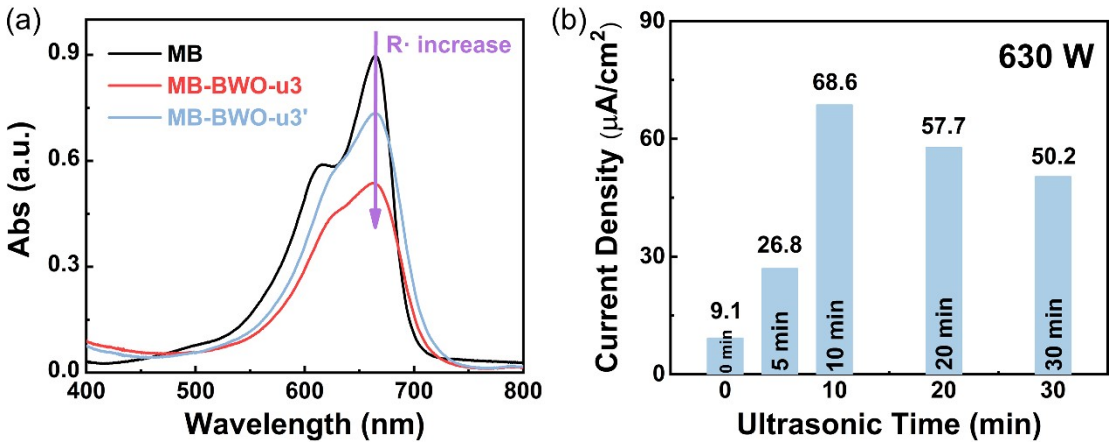

Fig. S3 (a) UV-vis spectra in reaction solution. (b) Photocurrent density of photoanodes treated under different ultrasonic time.

As shown in Fig. S3b, different from the direct acoustic cavitation regulation on surface, the ultrasonic time mainly affects the reaction degree. When less than 10 min the photocurrent density is intensified with the extension of time. The decline afterwards may originate from the emerging of bulk defects inside the Bi_2WO_6 lattice which hinder charge transmission.

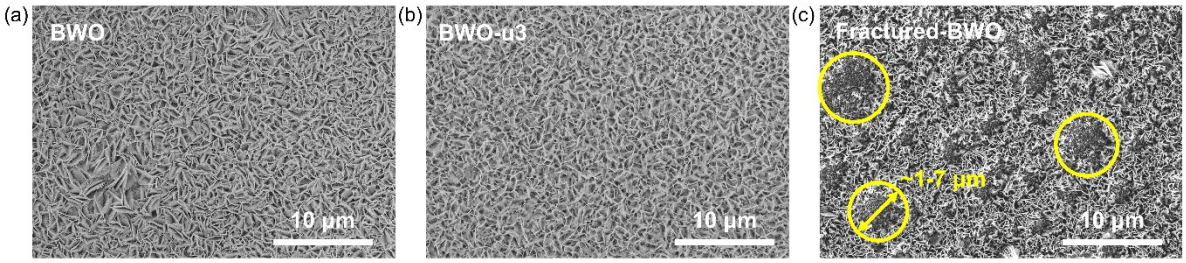

Fig. S4 SEM image of (a) BWO, (b) BWO-u3 and (c) fractured-BWO under excessive cavitation intensity.

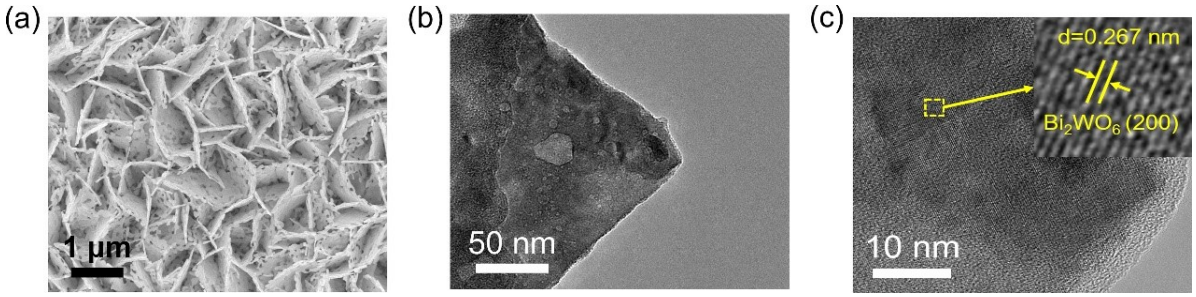

Fig. S5 (a) SEM image and (b-c) TEM image of BWO. (Illustration in (c): HRTEM image of BWO).

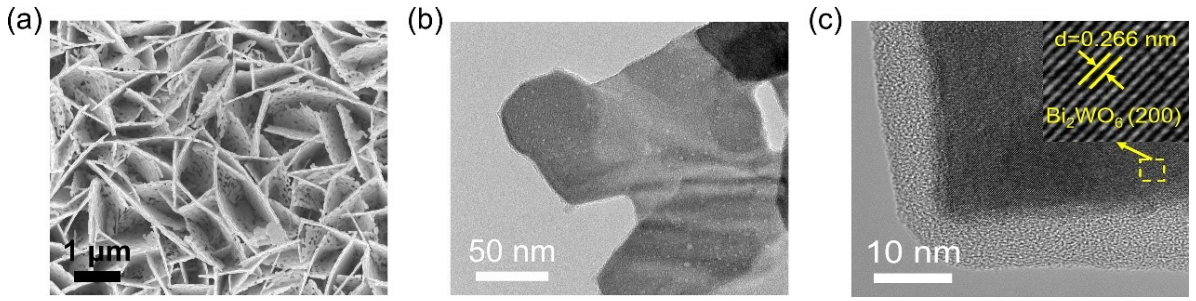

Fig. S6 (a) SEM image and (b-c) TEM image of BWO-u0. (Illustration in (c): HRTEM image of BWO-u0).

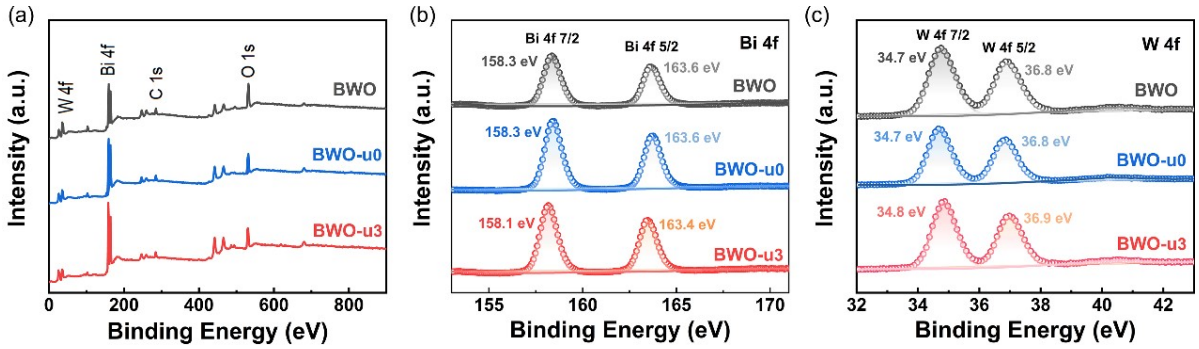

Fig. S7 XPS spectra of BWO, BWO-u0 and BWO-u3. (a) Survey, (b) Bi 4f, and (c) W 4f.

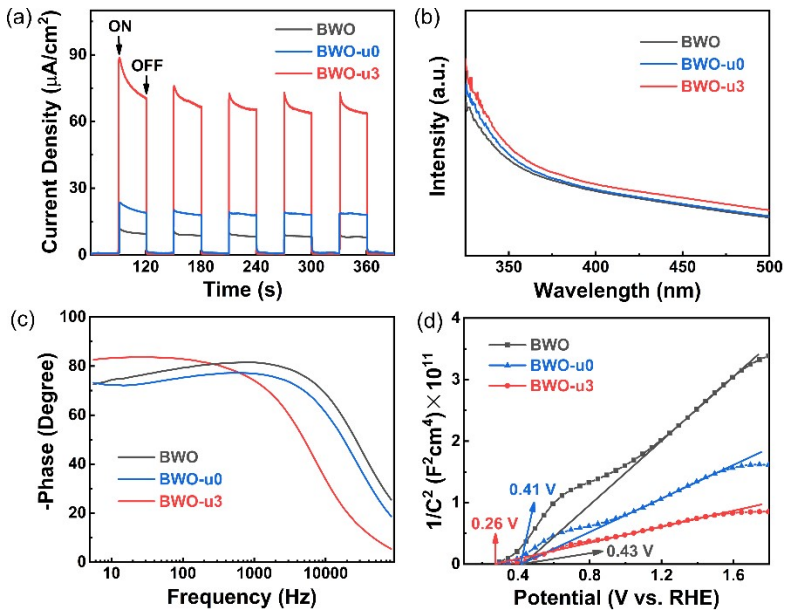

Fig. S8 (a) Amperometric i-t curves, (b) UV-vis spectra, (c) bode plots and (d) Mott-Schottky curves of BWO, BWO-u0 and BWO-u3.

To evaluate the charge separation and injection efficiencies in BWO photoanodes, Na_2SO_3 was added into the electrolyte as hole scavenger to participate in redox reaction with photogenerated holes to make sure that photogenerated electrons could not recombine with holes and participate in circuit transmission.[1] The linear voltammetry curves of BWO，BWO-u0 and BWO-u3 photoanodes are tested under irradiation of solar simulator. Charge separation efficiency η_{sep} and injection efficiency η_{inj} can be calculated by Eq. 3-4:

$$\eta_{sep} = J^{Na_2SO_3}/J_{abs} \quad (3)$$

$$\eta_{inj} = J^{H_2O}/J^{Na_2SO_3} \quad (4)$$

The TRPL curves of BWO，BWO-u0 and BWO-u3 photoanodes are fitted by bi-exponential decay and the detailed fitting parameters are listed in Table S2. The average lifetime (τ) is calculated by Eq. 5:

$$\tau = \frac{\sum A_i \tau_i^2}{\sum A_i \tau_i} \quad (5)$$

Where A_i (i = 1, 2) are the weighting coefficient and τ_i (i = 1, 2) are the characteristic lifetimes

of components.[2]

The Bode plot is shown in Fig. S8b, BWO-u3 displayed a negative frequency of characteristic peak, according to the Eq. 6:

$$\tau(lifetime) = \frac{1}{2\pi f_{max}} \quad (6)$$

Where f_{max} is the frequency maxima, revealing that the photogenerated carriers of BWO-u3 photoanode have a longer lifetime in the process of oxygen evolution reaction.

Through linear fitting of Mott-Schottky curves (Fig. S8c), the flat-band potential (V_{CB}) of BWO, BWO-u0 and BWO-u3 can be obtained, which are 0.43, 0.41 and 0.26 V (vs. RHE), respectively. The negative shift of flat band potential reveals the enhancement of charge transfer ability in BWO-u3 and the positive slope certifies the n-type semiconductivity of BWO.[3,4] The carrier density can be calculated as Eq. 7:

$$N_d = \left(\frac{2}{\varepsilon\varepsilon_0 q}\right)\left[\frac{d\left(\frac{1}{C^2}\right)}{dV}\right]^{-1} \quad (7)$$

Where C is the specific capacitance, q is the amount of electron charge, ε is the relative permittivity of the material, ε_0 is the vacuum permittivity, and V is the applied bias. A smaller slope of the linear part proves a significant improvement of photogenerated carrier density in BWO-u3 photoanode. The surface Vo serve as electron doners to make the surface carriers transmission more efficient, thus achieving better PEC performance.

Tabel S2. TRPL fitting parameters of BWO, BWO-u0 and BWO-u3 photoanodes.

Sample	τ_1(ns)	A_1(%)	τ_2(ns)	A_2(%)	τ(ns)
BWO	1.2880	39.71	14.3960	60.29	9.1910
BWO-u0	1.1919	44.60	16.0033	55.40	9.3978
BWO-u3	1.0422	31.23	18.7687	68.77	13.2321

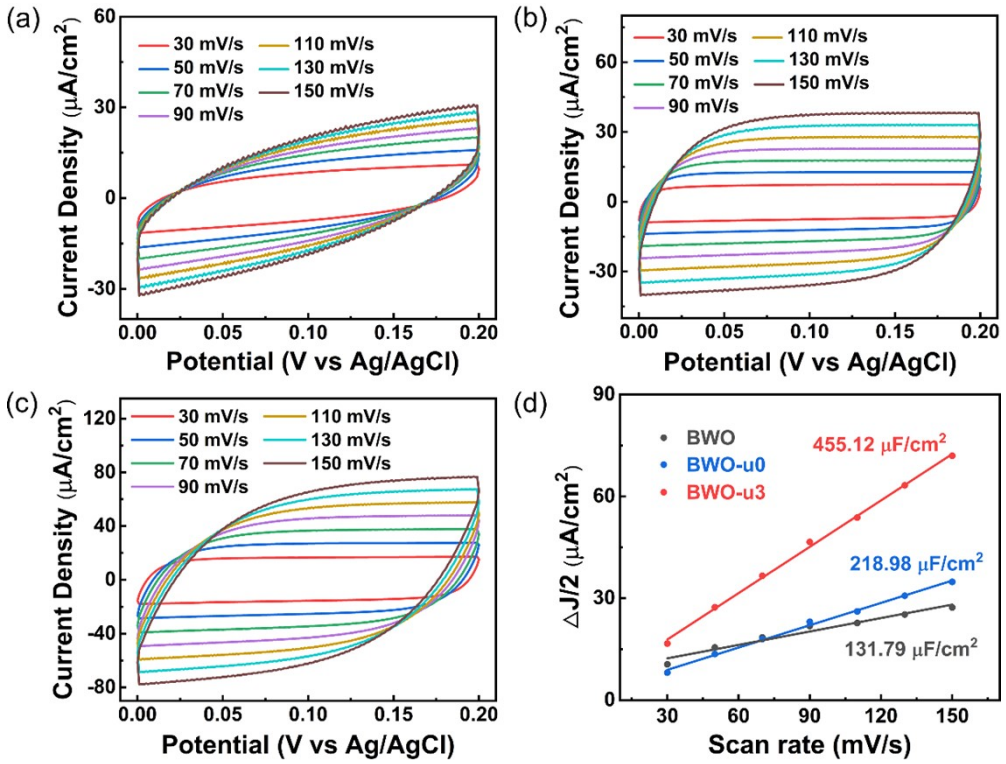

Fig. S9 Cyclic voltammetry curves with different scan rates of (a) BWO, (b) BWO-u0, (c) BWO-u3 photoanodes. (d) C_{dl} of three photoanodes.

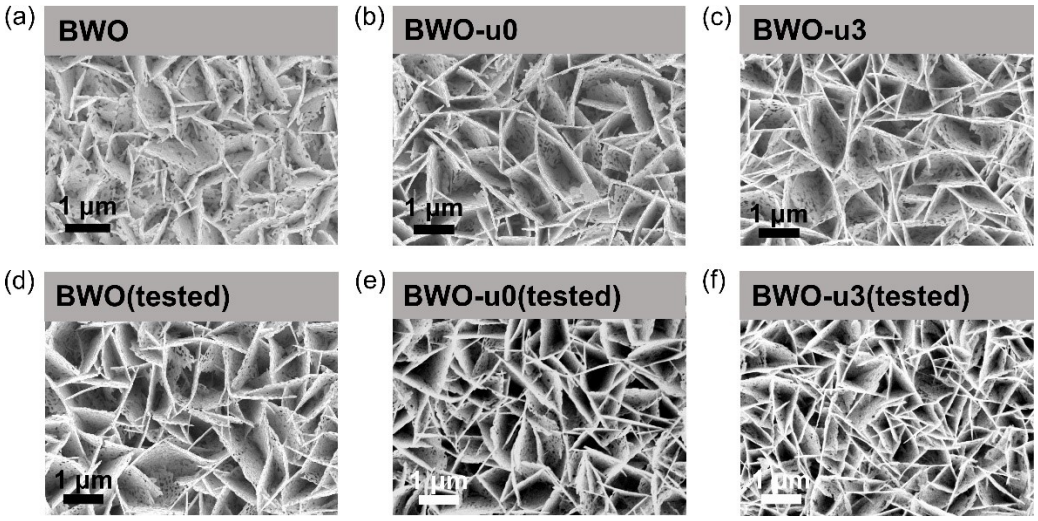

Fig. S10 SEM images of BWO, BWO-u0, BWO-u3 photoanodes before and after PEC tests. (a)(d) BWO, (b)(e) BWO-u0 and (c)(f) BWO-u3.

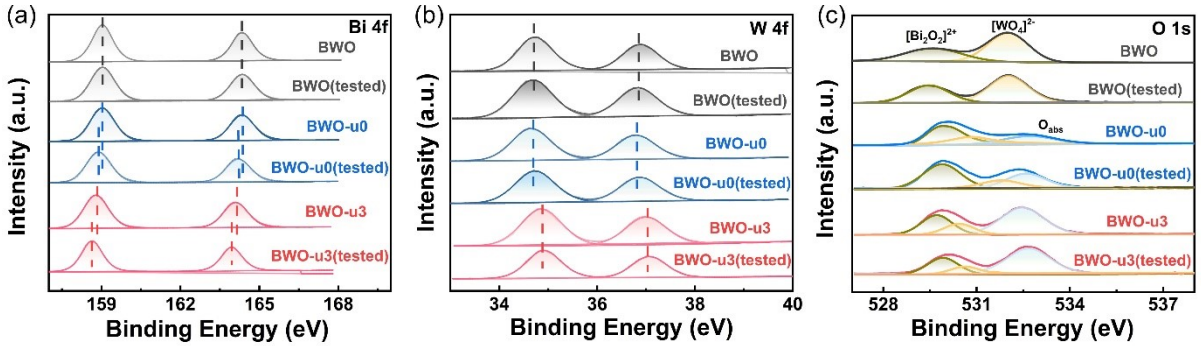

Fig. S11 XPS spectra of BWO, BWO-u0, BWO-u3 photoanodes before and after PEC tests. (a) Bi 4f, (b) W 4f and (c) O 1s.

To investigate the possible reasons of the decrease in photocurrent density of photoanodes, the SEM and XPS measurements of before and after long-term stability test are applied. No variation in SEM images is observed in Fig. S10 illustrates the stability of morphology on macroscopic scale. In Fig. S11, BWO, BWO-u0, and BWO-u3 are represent the surface states of untested photoanodes while BWO(tested), BWO-u0(tested), and BWO-u3(tested) are refer to the tested photoanodes. The binding energies of Bi 4f in BWO-u0(tested) and BWO-

u3(tested) photoanodes shows blue shift about 0.1 eV after 4 h PEC process as shown in Fig. S11a, which probably attributed to the electron accumulation at neighboring Vo during OER process, the barely change in the percentages of O_{abs} in Fig. S11c demonstrates the stability of Vo on BWO-u0 and BWO-u3 photoanodes.

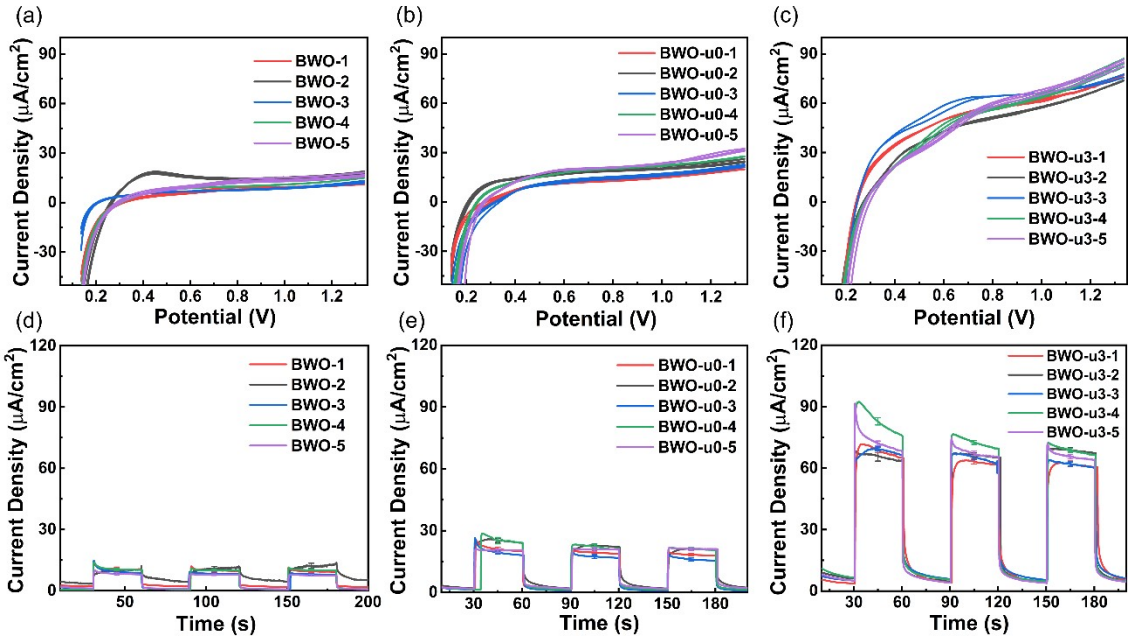

Fig. S12 The reproducibility of the BWO, BWO-u0 and BWO-u3 photoanodes. Linear sweep voltammograms curves of repeated (a) BWO, (b) BWO-u0 and (c) BWO-u3. Amperometric i-t curves of repeated (a) BWO, (b) BWO-u0 and (c) BWO-u3.

References

1 H. Chai, S. Wang, X. Wang, J. Ma and J. Jin, *ACS Catal*, 2022, **12**, 3700-3709.

2 G. S. Selopal, M. Mohammadnezhad, L. V. Besteiro, O. Cavuslar, J. Liu, H. Zhang, F. Navarro-Pardo, G. Liu, M. Wang, E. G. Durmusoglu, H. Y. Acar, S. Sun, H. Zhao, Z. M. Wang, F. Rosei, Adv. Sci., 2020, **7**, 2001864.

3 E. Blasco-Tamarit, B. Solsona, R. Sánchez-Tovar, D. García-García, R. M. Fernández-Domene and J. García-Antón, *J. Electroanal. Chem.*, 2021, **897**, 115579.

4 P. Zou, Z. Li, P. Jia, G. Luo and C. Wang, COLLOID SURFACE A, 2021, **623**, 126705.